MSUCL-241
May 1977

Cryogenic Helium Jet and Recoil Time-of-Flight Apparatus*

R.G.H. Robertson+

Department of Physics, Princeton University,
Princeton, New Jersey 08540, U.S.A., and
Cyclotron Laboratory, Michigan State University,
East Lansing, Michigan 48824, U.S.A.**

T.J. Bowles*** and S.J. Freedman++
Department of Physics, Princeton University,
Princeton, New Jersey, 08540, U.S.A.

An apparatus is described in which cyclotron-produced radioactivities are transported from the target area to a detection area in a stream of helium cooled to 92K. The apparatus is intended for investigations of β-delayed particle-emitting nuclei and includes a time-of-flight path which allows mass identification of the nucleus responsible for each particle group. A theoretical model for the transport of atoms in pure gases is presented which explains quantitatively many aspects of existing data both at room temperature and at low temperatures.

*Research supported by the U.S. National Science Foundation.

+Alfred P. Sloan Foundation Fellow.

**Present address.

***Present address: Physics Division, Argonne National Lab., Argonne, Illinois.

++Present address: Dept. of Physics, Stanford University, Stanford, California.

I. INTRODUCTION

The helium-jet technique[1] for rapidly transporting radioactive atoms from their point of production to another point has been much refined and improved since its inception. Until recently, it was thought that the addition to the the helium of impurities, such as organic vapors or aerosol dispersions of micrometer-sized particles, was essential to high transport efficiency, and indeed efficiencies near unity have been reported.[2] However, in some applications the presence of macroscopic amounts of non-volatile material in the gas stream is an undersirable or intolerable disadvantage. Such applications include the interfacing of the helium jet to certain types of ion source for mass spectrometry, precise studies of β-spectra, high-resolution measurements of delayed heavy-particle emission, and fundamental weak interaction studies which utilize the detailed spectral shapes of β-delayed particle lines. The particular application to which the present work is addressed is the extension of the limits of known radioactive nuclei to more proton-rich species, such as the T_z=-2 nuclei ^{20}Mg, ^{24}Si, ^{28}S, etc. That series of nuclei is expected to be characterized by β-delayed proton emission, which may permit location of the T=2 state in the daughter nuclei, and a test of the isobaric multiplet mass equation to unprecedented precision. In addition, the β-delayed proton emission affords a means of measuring the mass number of the precursor, a vital step in the identification of a new nuclide in the presence of other, much more abundant nuclides. As will be explained below, exploitation of this scheme depends on continuous preparation of an extremely thin source.

Helium jet systems have been operated successfully with "pure" helium, particularly over short transport distances, but have generally been characterized by very low efficiencies and non-reproducible behavior. In addition, even with "pure" helium, sufficient impurities are usually present that the problems associated with impurity-loaded systems remain. Recently, however, a group at the University of Jyväskylä have conducted systematic studies of helium jets operated with very pure helium and, still more significantly, have discovered that dramatic increases in efficiency are possible if the entire source volume is cooled to the temperature of liquid air.[3-5]

In the present paper a complete system associated with the Princeton University Cyclotron is described, in which a cryogenic (liquid-nitrogen cooled) helium jet is coupled to a recoil time-of-flight mass analyzer. Observations of some factors affecting transport efficiency are reported.

II. HELIUM JET SYSTEM

A. Theory of Operation

In 1973 Äystö and Valli published[3] a very detailed series of observations on the absolute efficiency of a simple helium jet system operated with "pure" commercial He at room temperature as a function of capillary length, capillary diameter, source pressure and capillary-catcher distance. The highly systematic behavior of the maximum observed transport efficiency for different choices of capillary length and diameter is perhaps not obvious in a casual inspection of their data, so, to make it clearer, those results are presented in Fig. 1. For a given capillary diameter, the efficiency is seen to have a characteristic exponential decrease with length after a very rapid drop in the first 20 cm. Increasing the capillary

diameter increases the over-all efficiency without materially altering the decay exponent. The maximum transport efficiencies observed by Äystö and Valli were always obtained at the same helium mass throughput, irrespective of capillary length or diameter. It should be pointed out that the results of Äystö and Valli are probably free of the uncertainty that usually accompanies measurements with "pure" helium (namely that sufficient impurities are always present to permit cluster formation) because there was no intense radiation in their apparatus, without which cluster formation is unlikely except in special circumstances.

In a second series of measurements, Äystö et al.[4] measured transport efficiencies with the source chamber and capillary cooled to the temperature of liquid air (80K), and found a dramatic increase over the efficiencies observed at room temperature. The data, which are presented in Fig. 2, are not quite as comprehensive as the room-temperature data, and seem to show a different type of behaviour as the capillary diameter is varied, although there are not really enough data points to ascertain the shapes of the efficiency curves.

To explain these observations a theoretical model will be presented in which the loss of active atoms during transport occurs entirely as a result of thermal diffusion towards, and adsorption by, the walls of the capillary. Such a model can quantitatively reproduce many features of the data shown in Figs. 1 and 2, including the strong temperature dependence of the efficiency. The importance of thermal diffusion in the transport of large clusters has been recognized by others[6,7] and Zirnheld[6] in particular has

found agreement between measured transport efficiencies for gold clusters and certain empirical formulas.

The concentration of atoms of type 1 in a gas of type 2 will, if ϕ is small, satisfy the well-known diffusion equation,

$$\frac{\partial \phi}{\partial t} = D_{12} \nabla^2 \phi ,$$

where D_{12} is the coefficient of thermal diffusion of gas 1 through gas 2. In a short region of capillary, the diffusion will have cylindrical symmetry, i.e.

$$\frac{\partial \phi}{\partial t} = D_{12} [\frac{1}{r} \frac{\partial}{\partial r} (r \frac{\partial \phi}{\partial r})]$$

Solutions to this equation have the form,

$$\phi = A \exp(-\lambda t) J_o(r \frac{\lambda}{D_{12}}),$$

where A is the concentration at t=0 and r=0, and $J_o(z)$ is the zero-order Bessel function. The boundary conditions are established by adsorption of the active atoms at the wall of the capillary.. The first zero of the Bessel function occurs at z=2.4, and for the moment no consideration need be given higher modes which will be quickly damped out by the exponential term. Thus,

$$\lambda = 5.76 D_{12} r_o^{-2}$$

where r_o is the radius of the capillary.

An expression for the diffusion coefficient D_{12} has been given by Jeans[8]:

$$D_{12} = \frac{2}{3(1+\alpha)\pi(\nu_1+\nu_2)S_{12}^2} [\frac{2kT}{\pi}(\frac{1}{m_1}+\frac{1}{m_2})]^{1/2}$$

Here m_1 and m_2 are the masses of the carrier and active atoms and ν_1 and ν_2 their molecular densities, S_{12} is the collision radius for the two species, and α is a small constant, always between 0 and 1/3. For the case of interest $\nu_1 \gg \nu_2$ and $m_1 \ll m_2$, and $\alpha = 1/3$. The molecular density ν_1 decreases and the flow velocity increases as the gas travels the length of the capillary. Let the transit time through an element of capillary Δx in length be Δt. Then

$$\lambda \Delta t = \frac{5.76}{r_o^2} \frac{2}{3(1+\alpha)\pi\nu(x)S_{12}^2} [\frac{2kT}{\pi}(\frac{1}{m_1}+\frac{1}{m_2})]^{1/2} \frac{\pi r_o^2 \Delta x}{q(x)}$$

where $\nu(x)$ is the molecular density (ν_2 has been neglected) and q(x) the volume flow rate at a point x. The molecular flow rate,

$$n_o \equiv \nu(x) q(x),$$

is independent of x under isothermal conditions. Integrating, one finds that the concentration of active atoms has a simple exponential dependence on the length of the capillary L, namely

$$\phi = \phi_o \exp(-\gamma L),$$

where

$$\gamma = \frac{2.30}{n_o S_{12}^2} [kT(\frac{1}{m_1}+\frac{1}{m_2})]^{1/2}. \qquad [1]$$

The predictions of this simple formula may now be compared to the experimental data.

(i) For a given flow rate n_o, the efficiency decreases exponentially with length, as is experimentally observed for lengths greater than 20 cm (see Fig. 1).

(ii) For a given flow rate, there is no dependence of the exponent on capillary radius, in accord with the data of Fig. 1.

(iii) Inserting values for the parameters appropriate to the experiments of Äystö and Valli,[3] $n_o = 2.0 \times 10^{21}$ sec^{-1}, $S_{12} = 5.6 \times 10^{-8}$ cm, T=300 K, $m_1 = 4$ amu, and $m_2 = 211$ amu, one finds excellent quantitative agreement with their room temperature data:

$$\gamma_{\text{theory}} = 2.77 \times 10^{-2} \text{ cm}^{-1}$$

$$\gamma_{\text{exp}} = 2.66 \times 10^{-2} \text{ cm}^{-1}$$

(iv) Equation 1 offers no explanation for the anomalously rapid drop in efficiency over the first 20 cm. Furthermore, it would appear that the efficiency could be arbitrarily inceased by increasing the flow rate n_o, whereas Äystö and Valli observed that, irrespective of capillary diameter or length, there was a maximum flow rate beyond which the efficiency decreased. Both of these phenomena are probably associated with turbulence near the capillary inlet. Another effect which can give a rapid initial decrease in intensity is the damping out of the higher mode solutions to the diffusion equation. However, depending on the boundary conditions at the entrance to the capillary, this decrease is only 30% or less and is independent of capillary radius.

(v) The temperature dependence of γ is moderate ($T^{1/2}$), but nevertheless, because γ is an exponent, very substantial changes in transport efficiency can occur as the temperature is changed. However, quantitative agreement with the 80-K data of Äystö, et al.[4] (Fig. 2) is not quite as satisfactory as with the 300-K data. The agreement for the 0.8 cm-diameter capillary is good,

$$\gamma_{\text{theory}} = 5.44 \times 10^{-3} \text{ cm}^{-1}$$

$$\gamma_{\text{exp}} = 6.44 \times 10^{-3} \text{ cm}^{-1},$$

but for the 1.0-mm and 1.2-mm capillaries, γ_{theory} is 2 and 3 times too large, repectively.

(vi) It is important to note that the enormous improvement in efficiency at low temperatures arises in equal measure from the four-fold decrease in T and the doubling of the molecular flow rate n_o. The critical flow rate observed by Äystö, et al.[4] is twice as large at 80 K as at 300 K.

(vii) It may also be remarked that some penalty in efficiency in transporting lighter atoms is to be expected from the factor S_{12}^{-2}.

(viii) No consideration in this theory is given to pressure diffusion, which, by virtue of the radial pressure gradient in the capillary, tends to oppose the effects of thermal diffusion. The deviations from quasi-static conditions are, however, relatively small except at the exit of the capillary, and it would appear that pressure diffusion is of minor importance in the cases considered here.

In summary, the general features of the transport of atoms by a pure gas are well described by the thermal diffusion model presented, and many

aspects are quantitatively explained. (This agreement in effect confirms that in the experiments of Äystö and Valli, both at room temperature and at 80 K, the atoms were indeed free and not attached to clusters). Guided by the theory, one may identify and optimize the important parameters of the helium jet system.

B. Apparatus

The helium jet target chamber consists of a large (20 x 15 x 15 cm) cell of 2 cm-thick welded aluminum plate. Commercial "pure" He (99.995 %) is passed through a liquid nitrogen (LN) trap, a section of room temperature pipe, and is then cooled again before entering the cell through a porous bronze diffuser. Considerable evidence was obtained with earlier designs that turbulence created by incoming gas could reduce or totally eliminate the transport of activities. With small cells or inlets too close to the thermalization region, very low efficiencies were observed, but if the He supply were pulsed on and off, the efficiency would often momentarily increase by orders of magnitude at the beginning of the "off" periods. A large volume cell and a diffusing element at the gas inlet prevent turbulence and allow continuous operation at high efficiency. The cell is in contact with LN, and isolated in a larger vacuum chamber. Beam passes through the cell via 0.05-mm Al windows. All flanges are sealed with indium wire.

The target projects into the beam inside the cell and recoil activities are extracted via a flared polyethylene capillary of 1.8 mm inside diameter located just behind the target. Two target-holder geometries were considered at the outset: one in which the target closed one end of a

cylinder through which He flowed axially until being drawn off by a capillary behind the target, and the second in which He was constrained to flow across the back of the target by a second foil parallel to the target but separated from it by 1 cm. Tests of the first geometry were made by injecting filaments of smoke into the gas flow, and it was observed that the region immediately behind the target was very poorly scavenged. Accordingly, the second geometry was adopted. It should be noted that when the nuclear half-life is comparable to the time it takes to scavenge the region behind the target there is no advantage in a multiple target assembly because the extra volume of gas needed to thermalize the recoils also increases the scavenging time. With the parallel-foil geometry, the calculated scavenging time is 50 ms for a He flow rate of 150 STP cm^3 sec^{-1}. The scavenging time is here defined as the ratio of the volume behind the target to the volume flow rate. However, measurements of the transport of nuclides (^{21}Mg and ^{25}Si) with different half-lives as a function of flow rate indicated that the effective time delay is longer than this, suggesting that there are substantial velocity gradients in the gas behind the target.

The large coefficient of expansion of plastics makes it difficult to achieve an effective vacuum seal to the capillary at LN temperatures. The capillary is therefore placed inside a thin-wall stainless steel outer tube which passes (via metal seals) between the cold cell and the vacuum vessel. The steel tubing is connected to plastic tubing which continues to enclose the capillary until it reaches the detection apparatus, where the temperature is high enough that a conventional O-ring seal is satisfactory. The capillary passes through a shielding wall 1 m thick and has a total length of 3.75 m.

A schematic illustration of the detection chamber is shown in Fig. 3. In a pure helium system, some attention must be paid to the gas flow in the region of the skimmer if good efficiency is to be maintained. The capillary enters a skimmer tube which is so constructed that axial symmetry is preserved for the gas deflected by the skimmer cone and pumped away. The skimmer cone full angle was chosen to be 90°, and the hole diameter is 2.1 mm. The skimmer tube is pumped by a 50 $\ell \cdot sec^{-1}$ Roots pump[9] backed by a 24 $\ell\ sec^{-1}$ two-stage rotary pump.[10]

Activities which pass through the skimmer are collected on a carousel of eight Formvar foils of 20 $\mu g\ cm^{-2}$ thickness and 6 mm diameter. The foils can be stepped from one position to the next by a rotary solenoid[11] in 35 ms. The detector chamber is pumped by a 260 $\ell\ sec^{-1}$ turbomolecular pump,[12] backed by a 24 $\ell\ sec^{-1}$ two-stage rotary pump.[10]

After an appropriate collection period, the foil carousel is stepped to place the activity in front of a Si detector. Protons (or α particles) pass through the foil and enter the Si detector. The residual nucleus is ejected in the opposite direction from the surface of the foil. These recoil fragments have sufficient energy to pass through a thin converter foil in front of a microchannel plate (MCP) assembly. The converter consists of 30 $\mu g\ cm^{-2}$ of Formvar supported on a 98%-transmitting Ni mesh. Electrons ejected from the converter are accelerated through a potential of 900 V to the front surface of the first channel plate. The use of the converter confers two advantages over the usual method of direct detection of the ions: first, the converter may be appropriately curved to reduce variations in ion flight path, and, second, the channel plates operate in an isolated, clean, high

vacuum (provided by a second turbomolecular pump[12]).

It may readily be shown that, if the time of flight is τ and the energy in the laboratory frame of the proton (or α particle) is $E_{p(lab)}$, then the mass of the daughter nucleus M_{rec} is given by:

$$M_{rec} = [2E_{p(lab)}m_p]^{1/2}\tau/d$$

where m_p is the proton (or α) mass, and d the flight path. The recoil mass is proportional to τ, not τ^2 as in the usual time-of-flight mass analyzer.

Successful application of this technique depends on a very low rate of transport of macroscopic impurity clusters in the helium jet, because the accumulation of material on the catcher foils can seriously degrade the energy resolution for the particles which must pass through the foil. The cryogenic helium jet meets this need very well: it was observed that the position and line-width of the 2.15-MeV α line from ^{20}Na decay remained fixed after days of continuous operation.

Several factors affect the time resolution (and hence the mass resolution). Since the proton decay is preceded by β-decay, the resulting initial recoil velocity causes a spread in the measured time of flight. In fact, for the cases of interest in the present work, this spread determines the mass resolution. For those decays which are pure Fermi transitions the electron-neutrino correlation is peaked at zero degrees and the corresponding recoil velocity is a maximum. Consequently it is not possible, with any flight path, to achieve better than, for example, 7% mass resolution in the decay of the lowest T=3/2 state of ^{25}Al. Nevertheless, the object is to provide mass identification, a key step in any search for new nuclides, and for this purpose

the mass resolution is adequate. Improved mass resolution is possible if β particles travelling in a certain direction are selected. Accordingly, an annular plastic scintillator is incorporated to detect β particles emitted into the same hemisphere as the recoil ions. Triple-coincidence data taken with this apparatus showed about 35% better mass resolution than the proton-recoil double-coincidence data.

The other factors which affect time resolution can be reduced to the level where they are unimportant compared to β-recoil. Electronic time resolution better than 1 ns is easily obtained. The converter solid angle is made as large as possible consistent with keeping the geometrical time dispersion due to finite source size unimportant compared to the effect of β-recoil. This results (for the nuclei considered here) in an 80-mm flight path and a 36-mm diameter converter. Monte Carlo calculations yielded an effective solid angle of 0.2 sr and a time spread of 2%, while the time spread due to β-recoil (for ^{25}Si decay) is 7% of the total flight time, 70 ns. Electron transit time spread from the converter foil to the channel plates is small.

The channel plates[13] were each 3.78 cm square, with 25 μm diameter channels at 15° to the normal. Electrical bias was supplied by the network shown in Fig. 4. Provision was made for recording the signals derived from the interface between the first and second channel plates. Some discrimination between single-electron or noise pulses and those arising from ions passing through the converter foil was possible using this signal.

III. EXPERIMENTAL RESULTS

Beams of 65 MeV ^{3}He ions from the Princeton University Cyclotron were degraded in energy to 58 MeV before reaching the target, 1 mg cm^{-2} of

99% enriched ^{24}Mg. The principal delayed-particle activities produced under these conditions are 445-ms ^{20}Na, 125-ms ^{21}Mg and 220-ms ^{25}Si. Some ^{8}B and/or ^{8}Li is also formed from carbon in the target. The ^{25}Si proved convenient for testing the apparatus. Although the total cross section for ^{24}Mg(^{3}He,2n)^{25}Si is not known at 58 MeV, it is estimated to be 50 μb, based on an extrapolation from lower-energy data[2,14] with the aid of the compound nuclear evaporation code ALICE.[15]

The transport efficiency was measured as a function of source chamber pressure and capillary-skimmer spacing. (Transport efficiency is defined in the usual sense and includes the efficiency for sweeping activities from the target cell and collecting them on catcher foils. Corrections for decay during scavenging, transport and collection, and for solid angle, have been been made). Figure 5 shows the efficiency measured for pure helium carrier gas. It was found that a six-fold increase in efficiency above these values could be obtained by the addition of 0.1% by volume O_2 gas. This increase in efficiency suggests the formation of simple molecules with the active atoms, thereby decreasing their thermal diffusion to the walls of the capillary and improving the action of the skimmer. A small change in the collision radius S_{12} can influence the transport efficiency greatly. Another possibility is the formation of droplets of liquid O_2, but the low partial pressure of oxygen makes this unlikely. It must be emphasized that, even if macroscopic clusters were being formed, they must have survived for only a brief time on the catcher foil, because the observations of the 2.15 MeV line from ^{20}Na decay mentioned above were made with the oxygen additive present.

At the operating pressure of 110 kPa (atmospheric pressure = 101 kPa) and a cell temperature of 92 K, a flow rate of 150 STP cm^3 sec^{-1} of helium is observed. Neglecting the increase in temperature along the capillary (which is cooled only by the flow of cold helium), and assuming for ^{25}Si atoms in He that $S_{12}=2.64 \times 10^{-8}$ cm one finds from equation [1]

$$\gamma_{theory}=3.74 \times 10^{-2}\ cm^{-1}$$

whereas $\gamma_{exp}=1.65 \times 10^{-2}\ cm^{-1}$,

In addition, no losses at the skimmer have been included in γ_{exp}. The smaller experimental loss coefficient is reminiscent of the results of Äystö, et al.[4] for the large-diameter capillaries.

Data were recorded on magnetic tape event-by-event for subsequent off-line analysis. Six parameters were recorded: MCP pulse height, Si detector pulse height, time of flight, time between Si detector and scintillator signals, time of event after a foil wheel step, and position of foil wheel. A mass spectrum was generated by using the prompt peak and the ^{25}Si recoil peak in the time spectrum as calibration points. Fig. 6 shows a small region of triple-coincidence data (in which coincidences between Si detector, MCP and scintillator are required), with proton energy on one axis and recoil mass (i.e. the atomic mass of the nuclide formed following proton emission) on the other. The principal activity is ^{25}Si, but broad lines from the decay of ^{21}Mg can also be seen. The rectangles indicate the regions in which protons following the β decay of ^{24}Si to the T=2 state in ^{24}Al are expected. The isobaric multiplet mass equation has been used to calculate the mass of the T=2 state, from which the energies for proton decay to the

ground and first excited states of ^{23}Mg can be estimated to a precision of ±14 keV. There is some positive indication of a group at the expected location of the ground state transition. It is clear that the technique holds considerable promise for the identification of new nuclides.

Spectra of β-delayed protons from ^{21}Mg and ^{25}Si, and β-delayed alphas from ^{20}Na, are shown in Fig. 7. These were obtained by setting windows on the appropriate mass regions in double-coincidence (particle-recoil) data. The energy resolution in the proton spectra is better than 20 keV, a figure that would be difficult to achieve with a detector telescope. The recoil time-of-flight technique permits particle identification with a single, high-resolution Si detector. For example, a new proton group at $E_{p(lab)}=(5.480 \pm 0.007)$MeV is resolved in the decay of ^{25}Si, and is the highest- energy proton branch from that nucleus. Its probable existence was suggested by Sextro[14] as the ground state branch from the lowest $\frac{3}{2}^+$ $T=\frac{3}{2}$ state in ^{25}Al at (7.972±0.003)MeV. The excitation energy from this work is (7.980 ±0.007)MeV.

The integral mass spectrum from double-coincidence data is shown in Fig. 8. Recoils from α-emitters (^8Li, ^8B, ^{20}Na) of course appear at half the recoil mass appropriate to proton emitters. The presence of tails (which may also be seen in Fig. 6) on the high-mass side of each peak is due to time signals from the channel plates arriving late. A possible explanation for a similar effect has been advanced by Zebelman et al.[16]: Primary electrons may dislodge secondary electrons from the surface of the front channel plate without producing a measurable signal. The secondary electrons then return to the channel plate slowly and cause a late time signal. The addition

of a grid in front of the first plate, biased positive with respect to it, was found by Zebelman et al. to eliminate the late tail, and such a modification will be included in this apparatus.

Figure 9 shows the integral pulse height spectra from the first channel plate for recoil ions of various masses and energies. The energetic ^{16}O recoils actually produce a recognizable peak in the spectrum, but low-energy ions produce only a featureless continuum. From the shapes of the latter spectra, it would appear that the detection efficiency is not unity, but, as shown in Fig. 10, for ions sufficiently energetic to pass through the converter foil at all, the detection efficiency is not a strong function of energy. The points in Fig. 10 were obtained by comparing the observed intensities of selected proton groups in the decays of ^{21}Mg and ^{25}Si with the measurements of Sextro,[14] and calculating the recoil range from the tables of Northcliffe and Schilling.[17] The estimated thickness of the Formvar converter foil was about 30 $\mu g\ cm^{-2}$. If 1-MeV ^{16}O recoils are detected with nearly 100% efficiency, then comparison of the peak heights of ^{20}Na and ^{25}Si lines in singles and coincidence spectra indicates an efficiency of about 50% for 170-keV ^{24}Mg recoils.

IV. CONCLUSION

The general behavior of helium jet systems operated with pure He can be understood in terms of a thermal diffusion model. The agreement with both room-temperature and liquid-air-temperature data is quite good, although it appears that a cryogenic system operated with a large diameter capillary is somewhat more efficient than predicted by the theory.

A liquid-nitrogen cooled helium jet coupled to a recoil time-of-flight analyzer has been constructed and tested with very satisfactory results. In addition to superlative cleanliness, the cryogenic system offers reliable and reproducible operation, at some cost in efficiency compared to cluster-loaded systems. It should be of great value in experiments which require a low level of macroscopic impurities.

V. ACKNOWLEDGMENTS

We wish to thank C.A. Gagliardi for his help in the construction of the apparatus, and assistance in many runs. We also extend our thanks to W.H. Moore for resolving, at unnatural times, difficulties with the operation of the cyclotron.

REFERENCES

1. R.D. Macfarlane and W.C. McHarris, in Nuclear Spectroscopy and Reactions, (ed. J. Cerny; Academic Press, New York, 1974), part A, p. 243.
2. H. Schmeing, V. Koslowsky, M. Wightman, J.C. Hardy, J.A. Macdonald, T. Faestermann, H.R. Andrews, J.S. Geiger and R.L. Graham, Nucl. Instr. and Meth. 139(1976)335.
3. J. Äystö and K. Valli, Nucl. Instr. and Meth. 111(1973)531.
4. J. Äystö, S. Hillebrand, K.-H. Hellmuth and K. Valli, Nucl. Instr. and Meth. 120(1974)163.
5. J. Äystö, V. Rantala, K. Valli, S. Hillebrand, M. Kortelahti, K. Eskola and T. Raunemaa, Nucl. Instr. and Meth. 139(1976)325.
6. J.P Zirnheld, Nucl. Instr. and Meth. 120(1974)171.
7. H. Wollnik, Nucl. Instr. and Meth. 139(1976)311.
8. Sir J. Jeans, Introduction to the Kinetic Theory of Gases (Cambridge University Press, Cambridge, 1962).
9. Leybold-Heraeus model R-152.
10. Leybold-Heraeus model DK-90.
11. Ledex model 216-612-023.
12. Welch model 3102A.
13. Galileo Electro-optics Corp.
14. R.G. Sextro, Ph.D. Thesis, University of California, LBL-2360 (unpublished).
15. M. Blann and F. Plasil (unpublished).
16. A.M. Zebelman, W.G. Meyer, K. Halbach, A.M. Pózkanzer, R.G. Sextro, G. Gabor, and D.A. Landis, Nucl. Instr. and Meth. 141(1977)439.
17. L.C. Northcliffe and R.F. Schilling, Nucl. Data Tables A7(1970)233.

FIGURE CAPTIONS

Fig. 1. Transport efficiency for ^{211}Pb in pure He at 300 K as measured by Äystö and Valli (Ref. 3). The dashed line is the prediction of the thermal diffusion theory presented in the text.

Fig. 2. Transport efficiency for ^{211}Pb in pure He at 80 K as measured by Äystö et al. (Ref. 4). The dashed line is the prediction of the thermal diffusion theory presented in the text. (Note the change in horizontal scale from Fig. 1.)

Fig. 3. Schematic diagram of the detector and recoil time-of-flight chamber.

Fig. 4. Biasing network for the channel plate detectors. The components shown are mounted in the vacuum chamber, close to the channel plates.

Fig. 5. Transport efficiency for ^{25}Si in pure He at 92 K measured with the apparatus described in the text. The normalization of absolute efficiency may be uncertain by as much as a factor of 2. The addition of a small concentration of O_2 gas increases these efficiencies substantially.

Fig. 6. A small portion of triple-coincidence data showing prominent bands from the β^+-delayed proton decays of ^{21}Mg and ^{25}Si. Proton energy increases linearly with channel number on the ordinate. The rectangles indicate the expected positions of proton groups from the unreported isotope ^{24}Si: There is some indication of a group at the location of the ground-state transition.

Fig. 7. Spectra of β^+-delayed proton decays of ^{25}Si and ^{21}Mg (top and middle, respectively) and, the α-decay of ^{20}Na (bottom). These were obtained from a single run by selecting the appropriate mass peaks. The instrumental energy resolution in the proton spectra is better than 20 keV.

Fig. 8. Integral mass spectrum computed from particle energies and time of flight. The apparent recoil mass of α emitters is half that of proton emitters. The tailing on the high mass side of the peaks is attributed to a spurious effect in the channel plate detectors (see text), while that on the low side of the ^{21}Mg peak is due to high energy protons which pass through the silicon detector.

Fig. 9. Pulse height spectra obtained from the interface between first and second channel plates for various ion species.

Fig. 10. Relative efficiencies for detecting low energy heavy ions as a function of their range in Formvar. The points without error flags are normalized to unity.

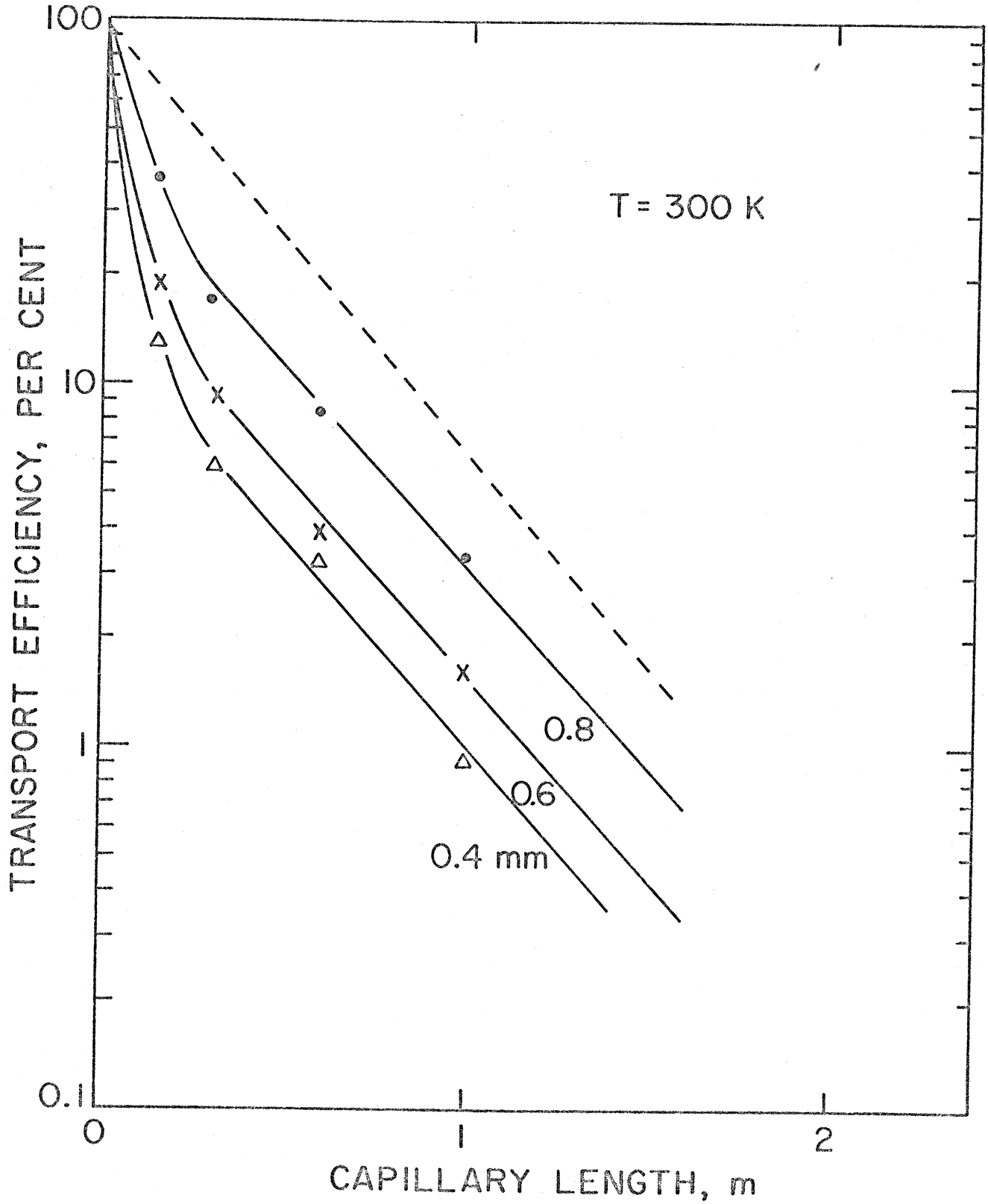
100
10
1
0.1
0
1
2
TRANSPORT EFFICIENCY, PER CENT
CAPILLARY LENGTH, m
T = 300 K
0.8
0.6
0.4 mm

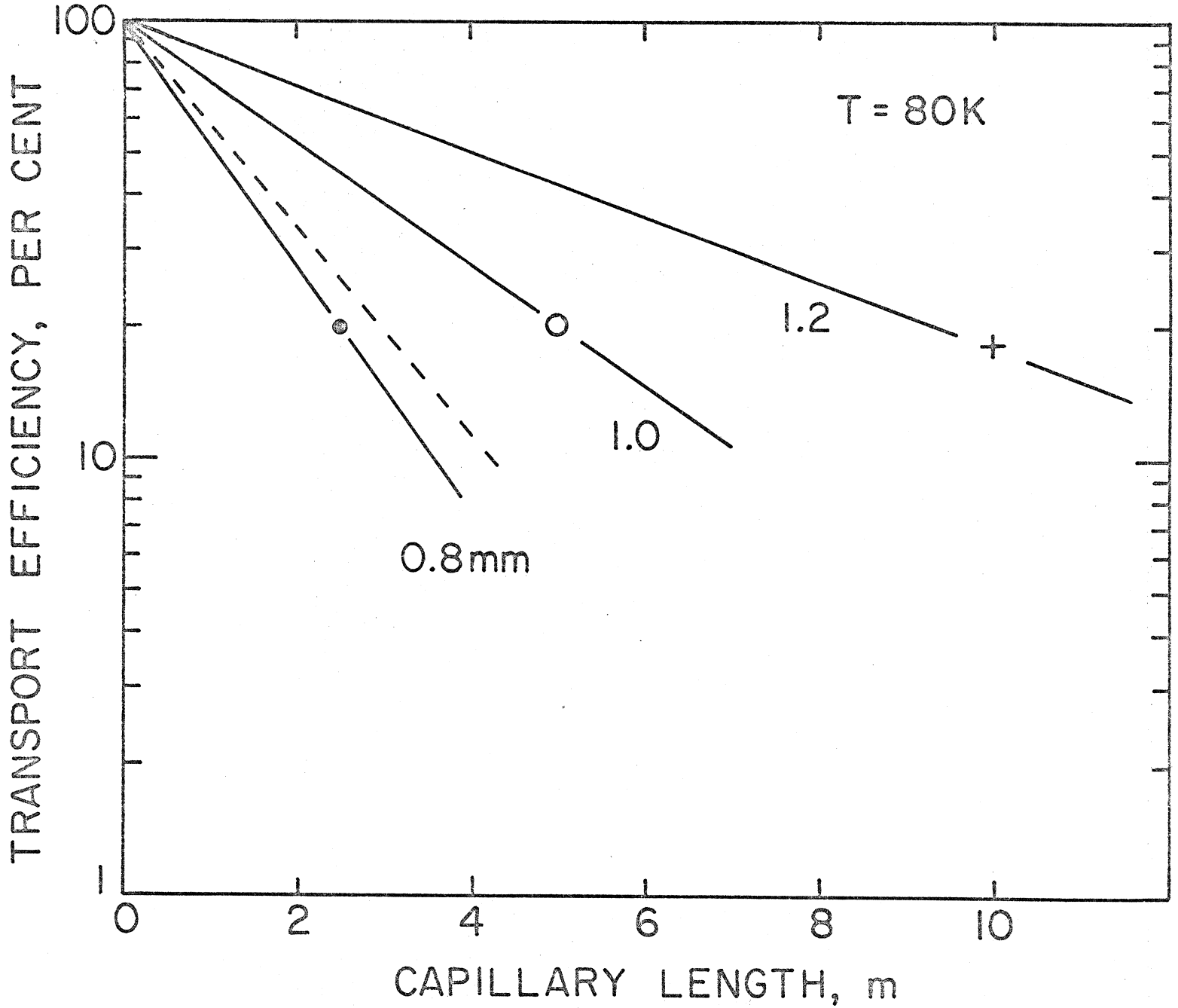
100
10
1
TRANSPORT EFFICIENCY, PER CENT
T = 80K
1.2
1.0
0.8mm
0
2
4
6
8
10
CAPILLARY LENGTH, m

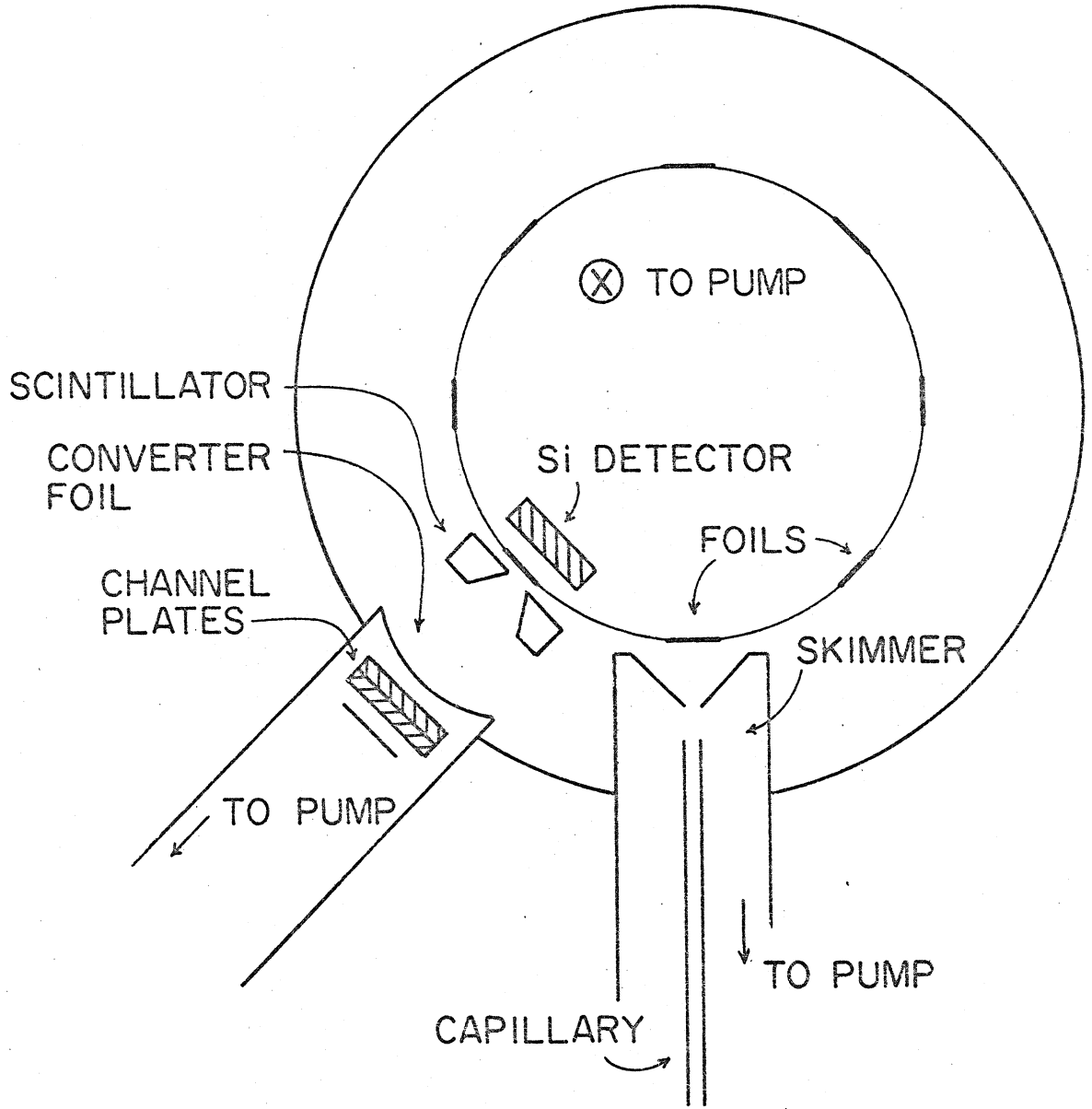
TO PUMP
SCINTILLATOR
CONVERTER FOIL
Si DETECTOR
FOILS
CHANNEL PLATES
SKIMMER
TO PUMP
TO PUMP
CAPILLARY

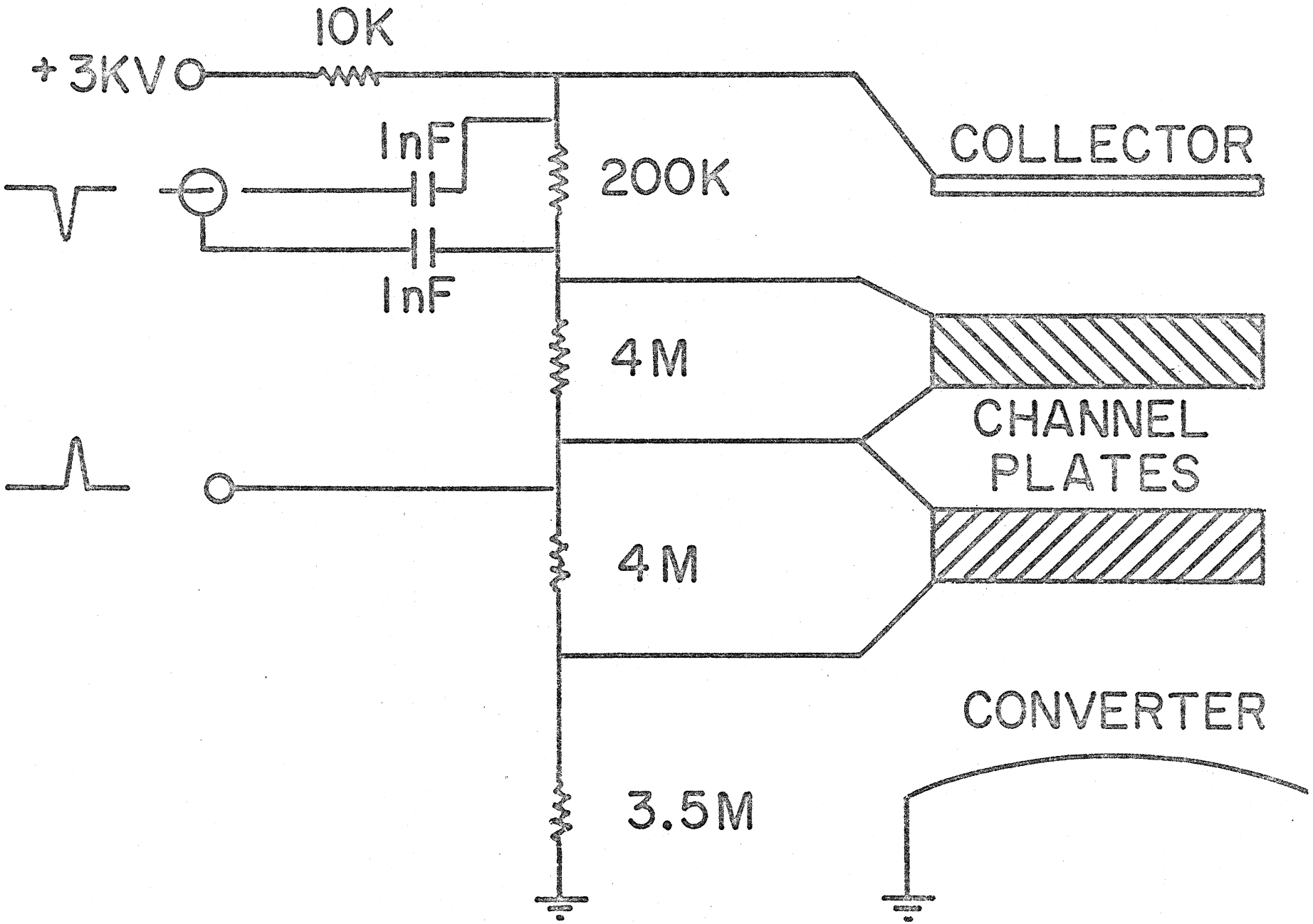
10K
+3KV
1nF
200K
COLLECTOR
1nF
4M
CHANNEL
PLATES
4M
CONVERTER
3.5M

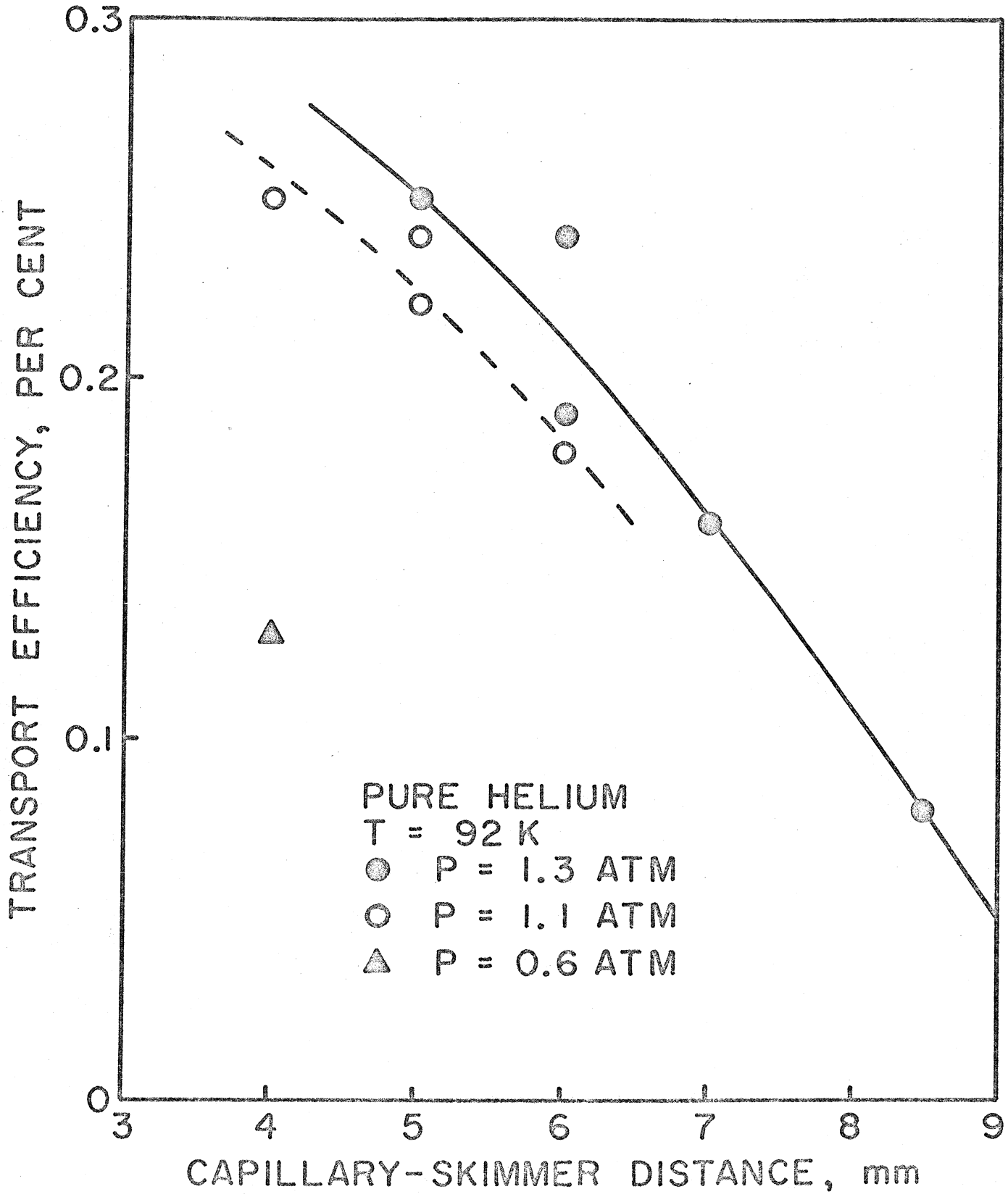
0.3
0.2
0.1
0
TRANSPORT EFFICIENCY, PER CENT
PURE HELIUM
T = 92 K
P = 1.3 ATM
P = 1.1 ATM
P = 0.6 ATM
3
4
5
6
7
8
9
CAPILLARY-SKIMMER DISTANCE, mm

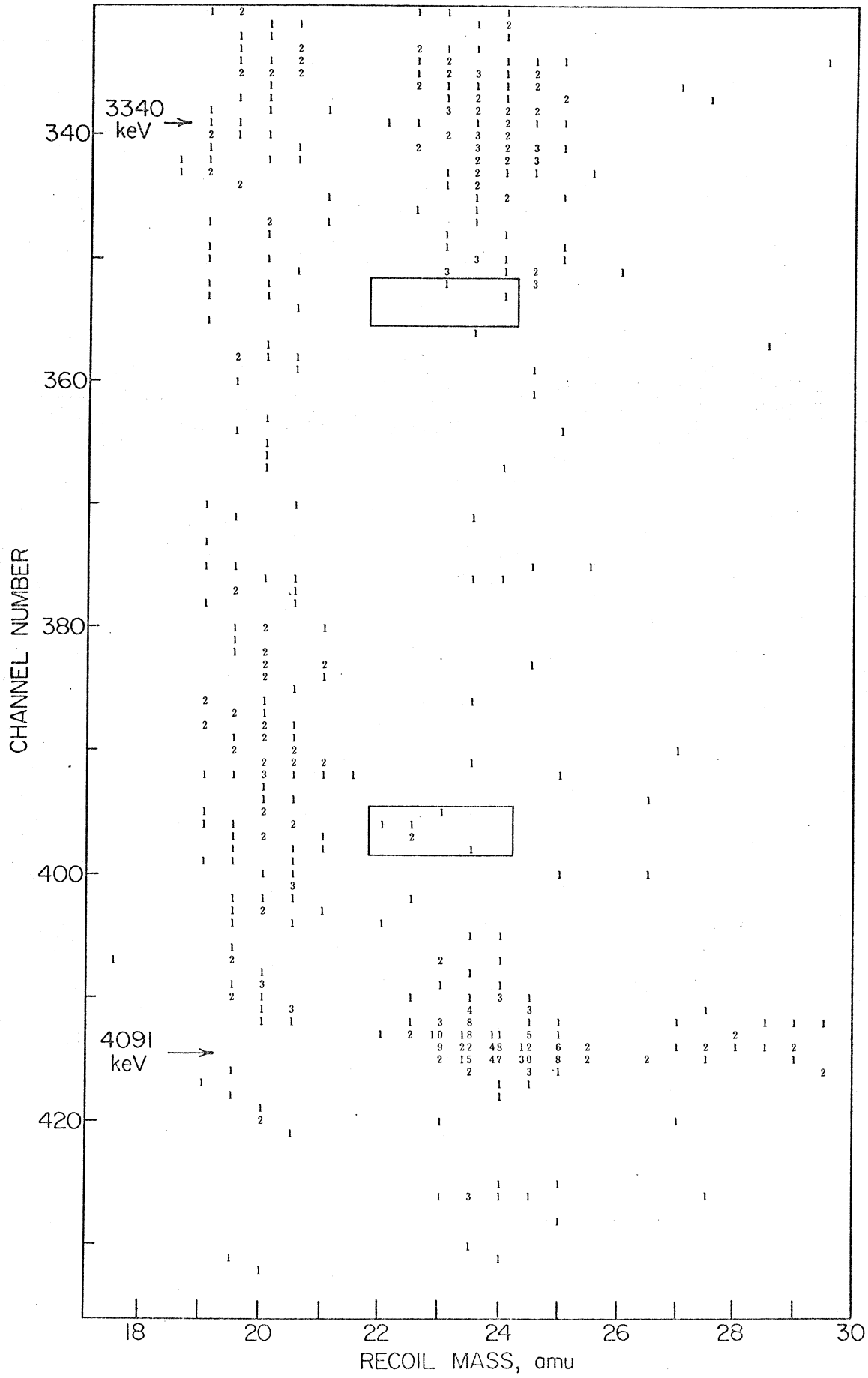
3340
keV
4091
keV
340
360
380
400
420
CHANNEL NUMBER
18
20
22
24
26
28
30
RECOIL MASS, amu

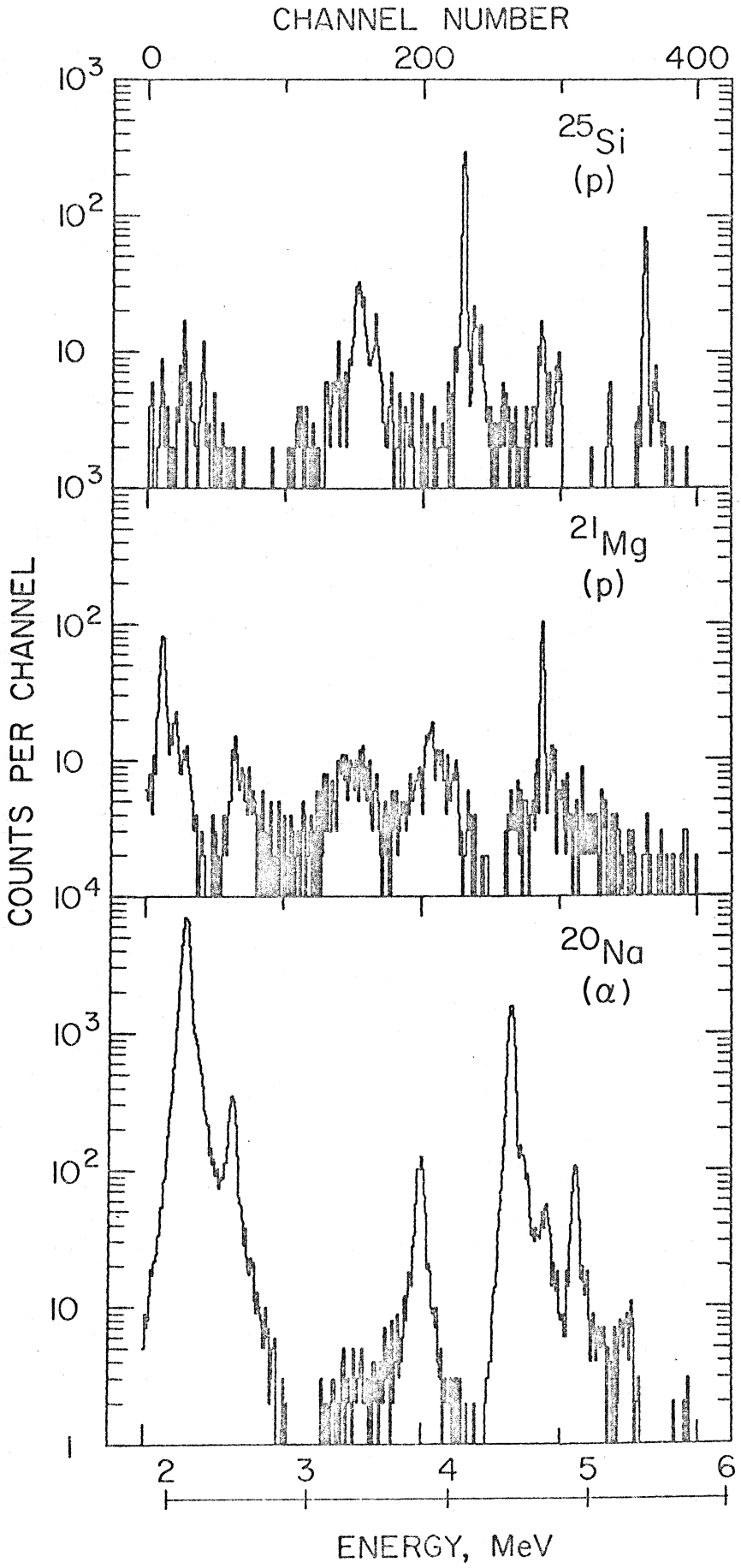
CHANNEL NUMBER
0
200
400
10^3
10^2
10
10^3
^{25}Si
(p)
10^2
10
10^4
^{21}Mg
(p)
10^3
10^2
10
1
^{20}Na
(α)
COUNTS PER CHANNEL
2
3
4
5
6
ENERGY, MeV

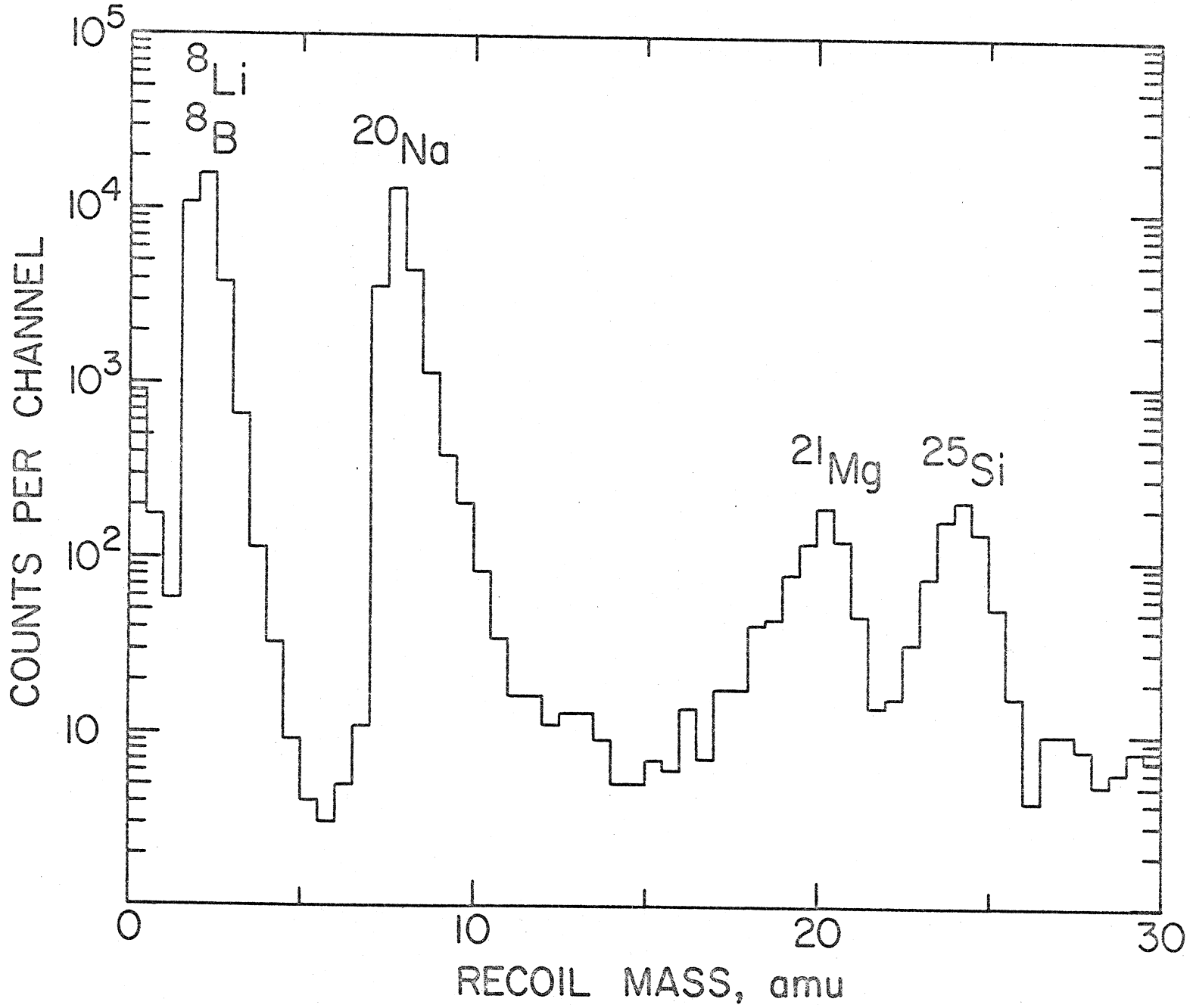
10^5
10^4
10^3
10^2
10
COUNTS PER CHANNEL
^{8}Li
^{8}B
^{20}Na
^{21}Mg
^{25}Si
0
10
20
30
RECOIL MASS, amu

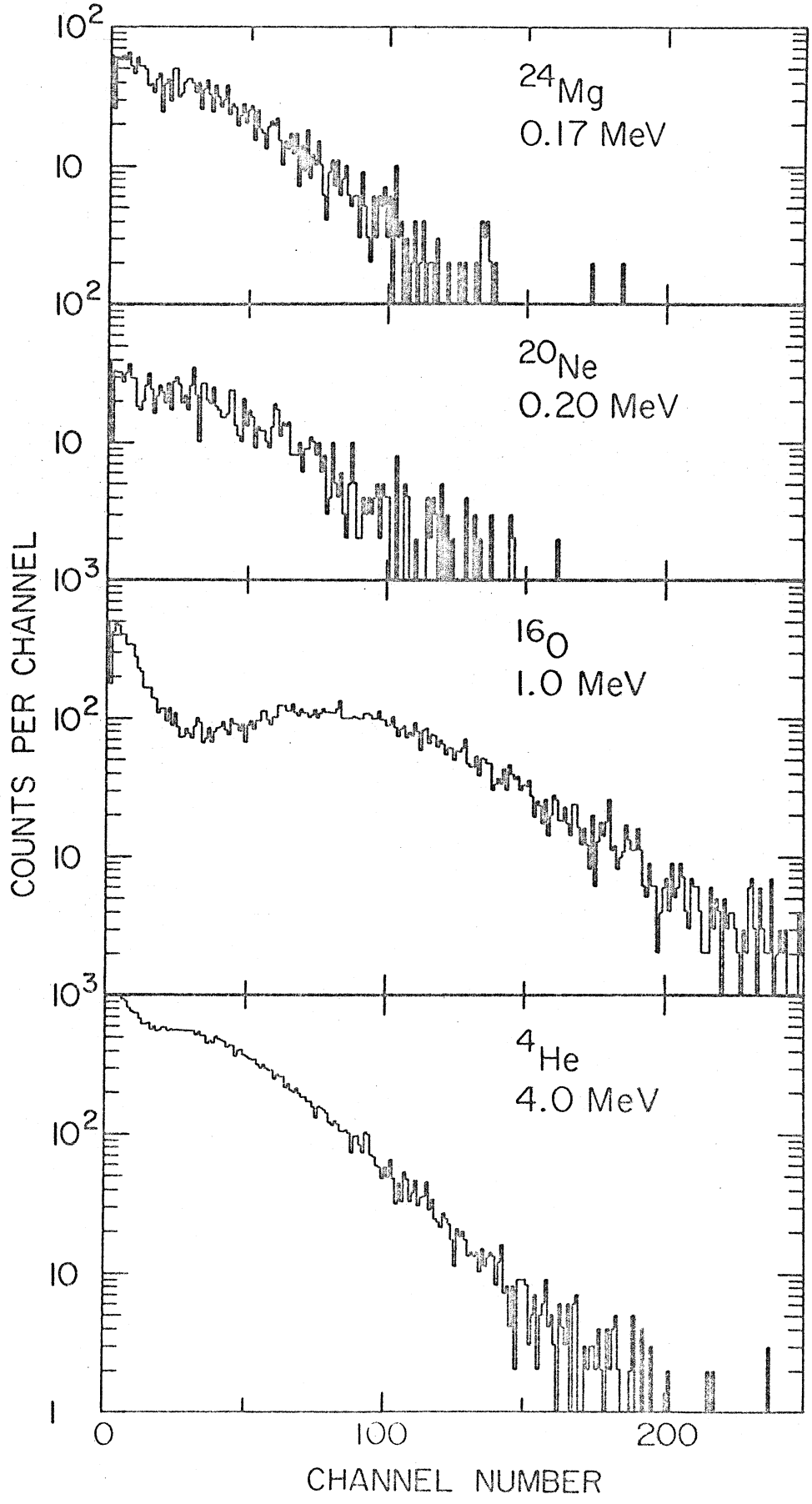
10^2
10
10^2
^{24}Mg
0.17 MeV
^{20}Ne
0.20 MeV
10
10^3
^{16}O
1.0 MeV
10^2
10
10^3
^{4}He
4.0 MeV
10^2
10
1
COUNTS PER CHANNEL
0
100
200
CHANNEL NUMBER

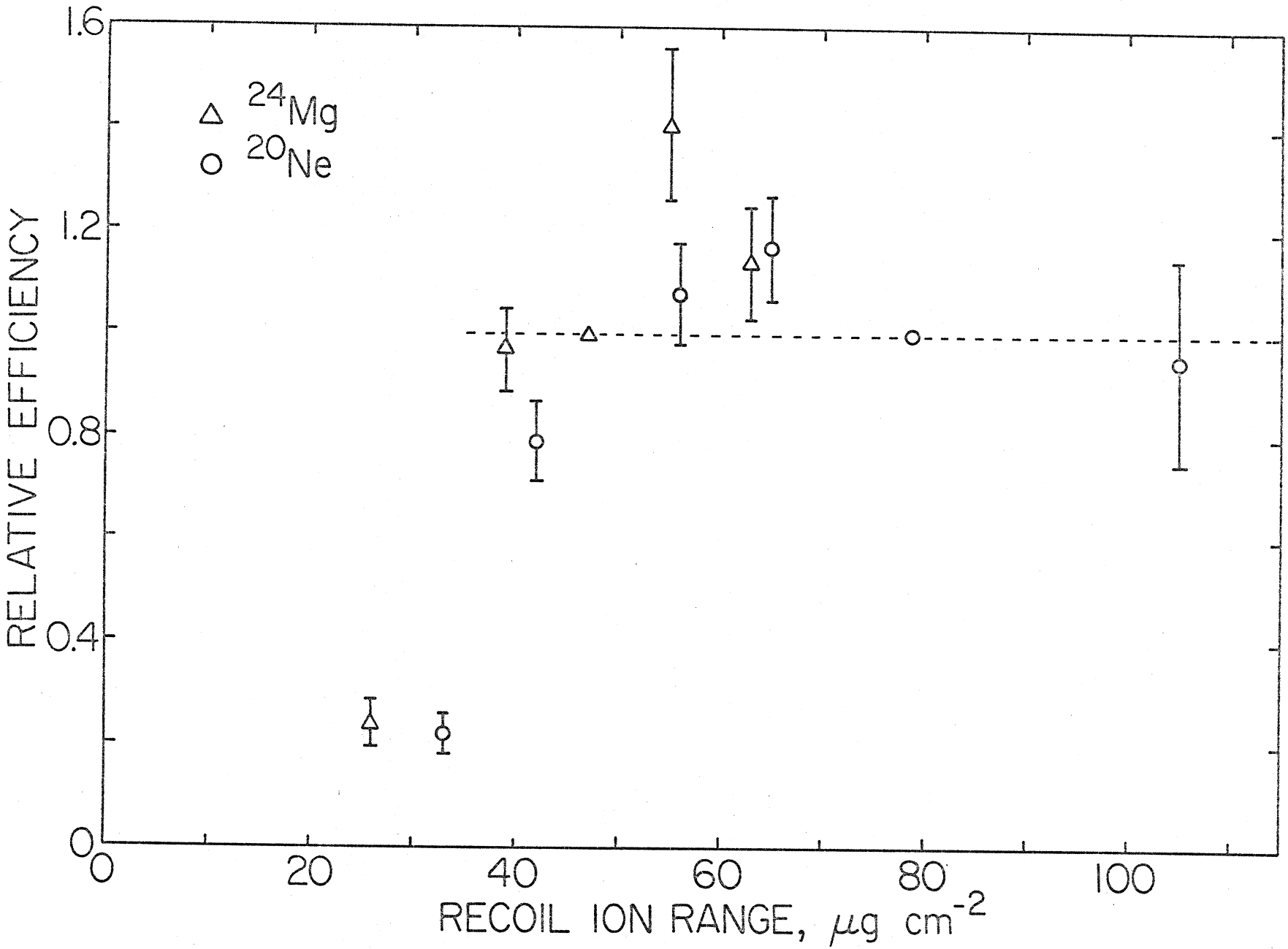
1.6
1.2
0.8
0.4
0
0
20
40
60
80
100
RELATIVE EFFICIENCY
RECOIL ION RANGE, μg cm⁻²
24Mg
20Ne